

High-resolution NIR Observations of the Circumstellar Disk System in the Bok Globule CB 26 ¹

B. Stecklum², R. Launhardt³, O. Fischer⁴, A. Henden⁵, Ch. Leinert³, H. Meusinger²

ABSTRACT

We report on results of near-infrared and optical observations of the mm disk embedded in the Bok globule CB 26 (Launhardt & Sargent 2001). The near-infrared images show a bipolar reflection nebula with a central extinction lane which coincides with the mm disk. Imaging polarimetry of this object yielded a polarization pattern which is typical for a young stellar object surrounded by a large circumstellar disk and an envelope, seen almost edge-on. The strong linear polarization in the bipolar lobes is caused by single scattering at dust grains and allowed to locate the illuminating source which coincides with the center of the mm disk. The spectral energy distribution of the YSO embedded in CB 26 resembles that of a Class I source with a luminosity of $0.5 L_{\odot}$. Using the pre-main-sequence evolutionary tracks and the stellar mass inferred from the rotation curve of the disk, we derive an age of the system of $\leq 10^6$ yr. $H\alpha$ and [SII] narrow-band imaging as well as optical spectroscopy revealed an Herbig-Haro object 6/15 northwest of CB 26 YSO 1, perfectly aligned with the symmetry axis of the bipolar nebula. This Herbig-Haro object (HH 494) indicates ongoing accretion and outflow activity in CB 26 YSO 1. Its excitation characteristics indicate that the Herbig-Haro flow is propagating into a low-density environment. We suggest

¹Based on observations carried out at the German Spain Astronomical Center Calar Alto, Spain, the Thüringer Landessternwarte Tautenburg, Germany, and the U.S. Naval Observatory, Flagstaff Station.

²Thüringer Landessternwarte Tautenburg, Sternwarte 5, D-07778 Tautenburg, Germany, stecklum@tls-tautenburg.de

³MPI für Astronomie, Heidelberg, Königstuhl 17, D-69117 Heidelberg, Germany

⁴AG Didaktik der Physik und Astronomie, Friedrich-Schiller-Universität Jena, Max-Wien-Platz 1, D-07743 Jena, Germany

⁵Universities Space Research Association/US Naval Observatory, Flagstaff Station, P.O. Box 1149, Flagstaff, AZ 86002-1149 USA

that CB26 YSO 1 represents the transition stage between embedded protostellar accretion disks and more evolved protoplanetary disks around T Tauri stars in an undisturbed environment.

Subject headings: accretion disks, polarization, ISM: globules, individual (CB 26), Herbig-Haro objects, individual (HH 494), stars: pre-main sequence, circumstellar matter

1. Introduction

Bok globules are small, opaque, and isolated nearby molecular clouds. Their cores usually have a quite simple structure which makes them ideally suited for studies of isolated low-mass star-formation (Bok 1977; Leung 1985). CB26 (Clemens & Barvainis 1988) was classified by Clemens et al. (1991) as quiescent, with little or no star-forming activity. The object was included in a comprehensive investigation of Bok globules using 1.3mm dust continuum and CS molecular line observations (Launhardt & Henning 1997; Launhardt et al. 1998) as well as near-infrared (NIR) imaging (Launhardt et al., in prep.). Launhardt & Henning (1997) found an unresolved 1.3mm source with $F_{1.3mm} = 160 \pm 14$ mJy slightly offset, but within the positional error ellipse from of IRAS 04559+5200 and concluded that a protostellar core is present in CB26. Recent interferometric observations by Launhardt & Sargent (2001) revealed that the major fraction of the thermal dust emission at mm wavelengths is due to a young, edge-on seen protoplanetary disk of diameter ~ 400 AU and mass $\sim 0.1 M_{\odot}$. They also suggest that CB26 is part of the Taurus/Auriga complex at the distance of 140 pc and thus nearer than claimed by Launhardt & Henning (1997). The revised distance will be adopted in the present paper.

Near-infrared (NIR) imaging of globules led to the detection of young stellar objects (YSOs) in many of them which are often associated with infrared reflection nebulae. One such example is CB 230 IRS which has a cometary shape due to light scattered in the northern (blueshifted) lobe of the outflow (Yun & Clemens 1994; Launhardt 2001). In such cases, the strong extinction even at NIR wavelengths prevents the direct view on the embedded pre-main sequence (PMS) star. However, it can be located using imaging polarimetry (e.g., Scarrott & Rolph 1991) since in the case of a single illuminating source, the polarization vector of single-scattered photons is perpendicular to the radius vector. The polarization pattern of YSOs is indicative for the dust properties and can often be explained by scattering in a circumstellar disk/envelope with bipolar cavities (e.g., Elsässer & Staude 1978; Fischer et al. 1994).

Our NIR imaging and polarimetry observations of CB 26 revealed the presence of an infrared source which is associated with the mm disk. In the following, we will refer to the embedded source in the globule as CB 26 YSO 1. This includes the NIR reflection nebula (called CB 26 IRS 1), the mm disk, and the central star.

2. Observations and data reduction

J, H, and Ks images were obtained using the MAGIC camera (Herbst et al. 1993) at the 3.5-m telescope of the Calar Alto observatory in 1994 January at the pixel scale of $0''.32$. The seeing was $\sim 1''$. The total field of view (FoV) of the mini mosaics is about $2'$. The total integration time of 800 s for each band led to 3σ surface brightness detection limits of 21.2, 20.5, and 20.1 mag/ \square'' . Astrometry was established using 5 stars in common with the Digitized Sky Survey 2 (DSS-II), yielding an accuracy of $\sim 0''.2$. Several photometric standard stars were observed during the night. Final flux densities listed in Table 1 were derived after background subtraction within synthetic circular apertures encompassing the entire NIR nebula.

CB 26 was re-observed in 1995 March using MAGIC together with a wire-grid polarizer at the pixel scale of $0''.07$ in the K band during sub-arcsecond seeing. The linear polarization (degree p and angle Θ) was derived from image stacks taken at four polarizer settings (position angles: 45, 90, 135, and 180°). Images at orthogonal directions were taken subsequently to minimize the effects of seeing and transmission variations. The total integration time per position angle was 200 s. The images were rebinned to $0''.28$ in order to gain signal-to-noise ratio. The K-band image shown in Fig. 2 is the sum of the four polarization frames. Its astrometry is based on our previous NIR images. Instrumental polarization was checked using standard stars from the UKIRT list and was found to be negligible compared to the high polarization degrees of CB 26 reported below.

Additional NIR imaging (H, K, L') was carried out using the 1.55-m Kaj Strand Astrometric Reflector of the USNO Flagstaff station together with ASTROCAM utilizing an ALADDIN 1024×1024 InSb array at the pixel scale of $0''.35$ in December 2000. Total integration times were 720, 720, and 180 s, respectively. The NIR images were processed using sky flats as well as bad pixel removal, and lastly mosaicked. HD 1160 served as photometric standard and was observed immediately before the science target at about the same airmass. Flux densities were derived in the same way as for the MAGIC images.

Optical images (I, H α) were taken with the 2048×2048 CCD prime focus camera of the 2-m Tautenburg telescope (diameter of the Schmidt correction plate 1.34 m) in February

2001 at the pixel scale of $1''.24$. Two exposures were done in each band with integration times of 180 s and 600 s, respectively, to enable the reliable removal of cosmic rays. The images were flat-fielded with dome flats and astrometrically calibrated using 8 stars from the DSS-II. Their spatial resolution is $\sim 4''$. Due to the larger bandwidth, the I-band image is 1.5 mag deeper than the $H\alpha$ frame. Since stars with known magnitudes are saturated on the I-band image, we established its photometry as follows. Ten stars from the USNO2 catalog (Monet et al. 1996) were selected which are in the unobscured neighborhood of the globule. Their I magnitudes were predicted using the (B–R) color as a guide for the spectral type. We found a good correlation between the predicted and the instrumental magnitudes, with a standard deviation of 0.3 mag sufficient for our purpose. Additional narrow-band imaging using the [SII] 6716/6731Å filter with an exposure time of 2×1200 s was obtained in September 2001.

Spectroscopy was performed in October 2001 with the newly commissioned Nasmyth spectrograph at the 2-m Tautenburg telescope using a total integration time of 1 hour and a slit width of $2''$, yielding a resolution of $\lambda/\delta\lambda \sim 960$. The wavelength calibration is based on night-sky lines. For this purpose, a template spectrum was generated by folding the Osterbrock Sky Spectrum¹ (www.nvao.org/NVAO/download/Osterbrock.html) to the observed resolution. The dispersion curve was derived by fitting a second order polynomial to the results of Gaussian fits to 14 lines in the wavelength region from 6200 Å to 7100 Å in both the observed and template spectrum. The zero point of this calibration was checked using the almost unblended [OI] 6300Å sky line which did not deviate by more than 5 km/s from the zero radial velocity which represents the 1σ uncertainty of the wavelength calibration.

An additional Nasmyth spectrum was obtained during good observing conditions in February 2004 using a $1''$ slit ($\lambda/\delta\lambda \sim 1800$) and an integration time of 20 minutes. During this run, the error of the wavelength calibration was checked by observing the brightest knot of the Herbig-Haro object (HHO) 366 for which Bally et al. (1996) found $v_{LSR} = +45$ km/s. Our estimate of $v_{LSR} = +42 \pm 3$ km/s agrees with their value and confirms the accuracy of the radial velocity estimation based on sky lines.

3. Results

Our NIR images reveal an infrared source (IRS1) close to the southwest rim of the small cometary-shaped Bok globule CB 26 (Figs. 1 and 3). Its morphology resembles that of bipolar reflection nebula. The central part of the nebula is bisected by a dark extinction lane

¹Preparation of the Osterbrock Sky Spectrum files was supported by grant No. ATM-9714636 from the NSF CEDAR program.

which is seen in the high-resolution NIR images (Figs. 1 and 2), but becomes most evident in the true color image shown in Fig. 3. The extinction lane is inclined at the position angle (P.A.) $55 \pm 7^\circ$, which is in good agreement with the P.A. of the mm emission from the circumstellar disk ($60 \pm 5^\circ$; Launhardt & Sargent 2001). A more diffuse and redder extension of the nebula stretching to the north-west is separated from the central part of the nebula by an additional, more diffuse extinction lane (Fig. 3, see also Sect. 4.1). The symmetry axis of the reflection nebula was derived from a weighted linear regression to the J-band brightness distribution clipped at the 3σ level. It is oriented along $\text{P.A.} = 144 \pm 1^\circ$, and is thus perpendicular to the plane of the disk and extinction lane. Since all three features, the reflection nebula, the extinction lane, and the mm disk are aligned within the small uncertainties, we assume a common symmetry axis along $\text{P.A.} = 145 \pm 5^\circ$.

Figure 2 shows our highest-resolution K-band image and the map of the linear polarization vectors. Single scattering yields high polarization degrees with the polarization vector perpendicular to the line connecting the illuminating source and the scattering grain. The most likely location of the illuminator was therefore derived by minimizing the mean square scalar product between polarization vectors with $p \geq 10\%$ and their corresponding radius vectors. This position is very close but not fully coincident with the center of the extinction lane. It is shifted by $0''.3$ to the north-west. However, the formal 1σ positional uncertainty of the center of illumination amounts to $0''.7$ (see Fig. 2) so that this displacement is not significant.

Area-integrated flux densities of the NIR reflection nebula were derived from aperture photometry in the calibrated images. Comparison of the H and K magnitudes from MAGIC and ASTROCAM images showed that they are consistent within ~ 0.1 mag. Because of the better signal-to-noise ratio, we use the MAGIC fluxes. The uncertainty of the L' flux is 0.5 mag. NIR flux densities of CB 26 YSO 1 and their errors, synthetic aperture diameters as well as beam sizes (stellar FWHMs due to seeing) are compiled in Tab. 1.

Our NIR photometry, the IRAS PSC as well as the submm/mm fluxes from Launhardt & Henning (1997), Henning et al. (2001) and Launhardt et al. (in prep.) were used to establish the spectral energy distribution (SED) of CB 26 YSO 1, shown in Fig. 6. The FIR to mm part of the SED was fitted by modeling the disk (parameters from Launhardt & Sargent 2001) plus a two-component spherical envelope consisting of cold (16 K) and warm (45 K) dust with a mass ratio of 750:1. A dust opacity $\kappa_\nu(1.3 \text{ mm})$ of $1 \text{ cm}^2 \text{ g}^{-1}$ together with a frequency dependence $\kappa_\nu \propto \nu^{1.8}$ was used for the envelope (Ossenkopf & Henning 1994). The best fit to the SED yields a total mass for the extended and slightly asymmetric envelope (see Henning et al. 2001) of $0.1 M_\odot$, which is comparable to the mass of the embedded disk (Launhardt & Sargent 2001). From the submm maps we estimate an average K-band

extinction through the envelope of order 1 mag. The NIR section of the SED was modeled by a modified 3000 K black body (typical for an M star), using an extinction curve from Rieke & Lebofsky (1985) and scattering efficiencies from Kim et al. (1994). No physical parameters were derived from the simple NIR fit. The mid-infrared part of the SED is very uncertain and not well-constrained by observations. Integration over 4π yields a luminosity L_{bol} of CB 26 YSO 1 of $0.47 \pm 0.04 L_{\odot}$, of which $\sim 5\%$ are from the NIR reflection nebula (i.e., due to emission/scattering at $\lambda < 12 \mu\text{m}$).

Figure 4 shows the wide-field I-band image of the region around CB 26. Overlaid are the contours of the continuum-subtracted $\text{H}\alpha$ image. An extended emission line feature is obvious $6'.15$ northwest of CB 26 IRS 1 which is also present on the [SII] image but lacks any continuum counterpart on the deeper I-band image. Its equatorial coordinates (J2000) are $\text{RA} = 04^{\text{h}}59^{\text{m}}29.^{\text{s}}4$, $\text{DEC} = +52^{\circ}09'52''$. The inspection of this region on the corresponding DSS-II-F plate digitized using the MAMA facility (Guibert 1992) shows a faint non-stellar object at the same location which is missing on the DSS-II-J image. Since the spectral response of the F plates almost peaks at $\text{H}\alpha$ while the J plates are not sensitive to this line, we conclude that it is the emission line object seen in our narrow-band frames.

The spectrum of this source is shown in Fig. 5. Strong emission lines ($\text{H}\alpha$, $\text{H}\beta$, [OI] 6300 \AA , [NII] 6584 \AA , [SII] 6717 \AA , and [SII] 6731 \AA) confirm its Herbig-Haro nature. This newly discovered HHO has the entry 494 in the catalog of (Reipurth 1999). The symmetry axis of the NIR reflection nebula and the mm disk (P.A. $145 \pm 5^{\circ}$) precisely points to the HHO (P.A. of the connecting line $147^{\circ}.5$), suggesting a physical connection between the two (see Fig. 4). The almost edge-on view of the circumstellar disk (Launhardt & Sargent 2001; see also Sect. 4.1) implies that the projected linear separation of 0.25 pc ($\approx 5 \times 10^4 \text{ AU}$) between CB 26 YSO 1 and HHO 494 is very close to the true separation. The radial velocity of HHO 494 was derived from the lines shown in Fig. 5 and amounts to $v_{\text{LSR}}^{\text{HHO}} = -45 \pm 7 \text{ km/s}$.

4. Discussion

4.1. Morphology of the disk and envelope

The morphology and SED of the embedded YSO resembles that of low-mass Class I source consisting of a PMS star surrounded by a circumstellar disk embedded in an envelope (e.g., Padgett et al. 1999; Zinnecker et al. 1999). While the embedded YSO is not seen directly due to high extinction in the surrounding disk, stellar light scattered at dust grains in the envelope below and above the disk becomes evident as bipolar NIR reflection nebula.

The observed centro-symmetric polarization pattern (Fig. 2) is caused by light scattering

in this bipolar geometry, resulting in very high values of $p \sim 50 \dots 90\%$ at the outer lobes due to single scattering. The linearly aligned polarization vectors close to the disk might be caused by back-scattering from the envelope onto the optically thick disk (Bastien & Ménard 1990) or by multiple scattering in the outer disk regions (Whitney & Hartmann 1993).

The central extinction lane which bisects the nebula is the signature of the disk. In the case of CB 26, this was directly demonstrated by spatially resolved mm observations of the thermal dust emission from the disk which precisely resembles the position, size, shape, and orientation of the extinction lane (Launhardt & Sargent 2001; see their Fig. 2). The disk must be seen almost edge on since none of the NIR lobes seems to be strongly shadowed. This is consistent with a preliminary model to the mm dust emission from the disk which suggests an inclination angle of $\lesssim 5^\circ$. An independent estimate of the disk inclination can be derived from the kinematics of the HHO (cf. Section 4.3). The morphology and colors of the NIR reflection nebula give no solid clue on which side of the disk might be tilted toward the observer. While the slightly brighter and bluer south-eastern lobe may indicate that this side is tilted toward the observer, the presence of the conical extension to the north-west (Fig. 1) and the possible small displacement of the center of illumination with respect to the center of the disk (Fig. 2) point toward the other direction. However, the displacement is within the range of the astrometric uncertainties and we cannot rule out that differences in the appearance of the bipolar lobes are due to varying extinction. Evidence for non-uniform extinction comes from an additional, more diffuse extinction lane between the compact north-western lobe and the more diffuse north-west extension of the NIR nebula which might be due to either an irregular shape of the remnant envelope or a foreground filament (see Fig. 3). The different resolution of the J, H, and Ks images due to the variation of the seeing precluded the derivation of dust grain properties from the wavelength dependence of the extinction lane and the observed polarization (cf., Wolf, Padgett, & Stapelfeldt 2003).

We also note that the south-western bright rim of the globule which is close to CB 26 YSO 1 coincides with a radio source that is present in 1.6 GHz and 4.85 GHz surveys (Gregory et al. 1996; Condon et al. 1994). The flux densities at these frequencies are 106 and 30 mJy, respectively, indicating a non-thermal origin. Thus, the radio source seems to be unrelated to CB 26.

4.2. The central illuminating star

Although the central illuminating star is not visible due to the high extinction, its presence and location could be unambiguously identified by means of the imaging polarimetry (cf. Sect. 3). Within the errors it is situated at the center of the mm disk.

The luminosity of CB 26 YSO 1 of $\approx 0.5 L_{\odot}$, which was derived by integrating the SED over 4π , is only a lower limit to the intrinsic luminosity of the embedded star since the bipolar geometry causes an anisotropic radiation field (Men'shchikov & Henning 1997) where, due to the edge-on view, only a fraction of the NIR photons are scattered into the line of sight. However, anisotropic radiation is not expected for the thermal FIR to mm emission, which contributes 95% to the total luminosity. Thus, even a very high anisotropy correction factor of 10 would increase the bolometric luminosity by only 50%. On the other hand, heating of such an isolated low-mass cloud core by the interstellar radiation field might not be negligible (e.g., Siebenmorgen, Kruegel, & Mathis 1992), resulting in an overestimation of the intrinsic luminosity of the embedded YSO. Together with the dynamic mass estimate for the PMS star by Launhardt & Sargent (2001) of $0.3 M_{\odot}$, a bolometric stellar luminosity of $\leq 0.5 L_{\odot}$ yields an upper limit for the age of 10^6 yr based on the solar-metallicity PMS tracks of Siess et al. (2000). From the SED we calculate a ratio $L_{\text{submm}}/L_{\text{bol}} \approx 2.5 \times 10^{-2}$ for CB26 YSO1. According to André et al. (1993) this ratio would be indicative of a Class 0 protostar since it is significantly higher than the threshold value 5×10^{-3} . However, this threshold value was derived from the assumption of spherical symmetry which does no longer hold for Class I YSOs. According to the morphology and age, CB26 YSO 1 is clearly a Class I object. The particularly large discrepancy in this case is most likely due to both the 'unusually' large and massive disk and the extreme edge-on view. This also demonstrates that a single parameter like the $L_{\text{submm}}/L_{\text{bol}}$ ratio cannot be used to unambiguously classify an individual source, although it may be useful to analyse (in a statistical sense) a larger sample of objects.

The IRAS non-detection at 12 and $25 \mu\text{m}$, which is non-typical for a Class I source, is most likely due to the extreme edge-on morphology and the resulting high extinction for the MIR emission from hot dust in the inner disk.

Since X-ray activity is a sign of low-mass YSOs (e.g., Feigelson & Montmerle 1999), we searched the ROSAT archive for a possible X-ray counterpart. Indeed, there are deep ROSAT images of this area but the superposition with the strong supernova remnant 1H 0455+518 (Pfeffermann et al. 1991) makes it difficult to detect CB 26 YSO 1.

4.3. The Herbig-Haro flow

The newly discovered HHO 494 is well aligned with the symmetry axis of CB 26 IRS 1, suggesting a physical relation between the two. There is no other star-formation activity in the region which could possibly be responsible for the Herbig-Haro flow. The neighboring globules CB 24 and CB 25 are quiescent and do not harbor any infrared sources seen in the 2MASS survey or by IRAS. The only other IRAS source in the vicinity is 04554+5210 to

the north-west, at about the same projected distance as 04559+5200. It is only detected at $100\ \mu\text{m}$ with a flux of 4.4 Jy and there is no evidence for star formation for this source. The absence of other possible driving sources for the Herbig-Haro flow in the field supports our view that HHO 494 is due to the outflow activity from CB 26 YSO 1.

The radial velocity of HHO 494 of $v_{LSR}^{HHO} = -45 \pm 7\ \text{km/s}$ is blueshifted with respect to the systemic radial velocity of the disk $v_{LSR}^{disk} = 5.5\ \text{km/s}$ (Launhardt & Sargent 2001). This indicates that the north-western lobe of CB 26 IRS 1 is tilted toward the observer. The assumption of a maximum disk inclination of 5° (cf. Sect. 4.1) leads to a velocity estimate of the Herbig-Haro flow of at least 500 km/s. Although such a flow velocity seems rather high, it is not uncommon for Herbig-Haro flows from Class I YSOs, e.g., HH 111 (Reipurth, Raga, & Heathcote 1992), HH 395 (Stecklum et al., in prep.) and consistent with the absence of a correlation between source luminosity and flow velocity (Reipurth & Bally 2001).

However, an independent estimate of the total flow speed can be derived from the detection of HHO 494 on the POSS-II-F and CCD narrow-band images. The epoch difference between these observations amounts to 4.4 yr. The positional coincidence suggests that any proper motion must be smaller than the pixel size of $\sim 1''$. With the assumption of a negligible proper motion of the mm disk, this yields an upper limit for the tangential velocity component of 150 km/s which implies an overall flow velocity of $\lesssim 160\ \text{km/s}$. Since this estimate of the tangential velocity is based on direct measurements, we prefer it over the value resulting from the radiative transfer model. Consequently, the disk inclination cannot be smaller than 18° if the jet is perpendicular to the disk, i.e. in the absence of any precession. When combined with the linear separation of the HHO from CB 26 YSO 1 the upper bound on the tangential velocity yields a lower limit for the dynamic time-scale of about 1600 yr.

Ratios of the emission line strengths are a good diagnostic of the excitation conditions, (e.g., Raga, Böhm, & Cantó 1996). The ratio of the [SII] 6717Å and 6731Å lines is insensitive to the electron temperature, thus allowing the determination of the electron density (Czyzak et al. 1998) which amounts to $n_e \sim 50\ \text{cm}^{-3}$. An upper limit for n_e of $230\ \text{cm}^{-3}$ is set by the signal-to-noise ratio of the spectrum. The ratio of the [NII] 6583Å and [OI] 6300Å lines is tracing the ionization fraction and almost independent of pre-shock density and magnetic field strength (Hartigan, Morse, & Raymond 1994). The derived value for the ionization fraction of 0.25 ± 0.05 implies a total gas density of about $200\ \text{cm}^{-3}$. This rather low density suggests that the Herbig-Haro flow is propagating into an environment more similar to the interstellar medium than a molecular cloud. At such densities the braking of the flow by the ambient medium is presumably not very efficient which might explain the observed high flow velocity. From the line ratio of [NII] 6583Å to [OI] 6300Å we also infer the shock velocity of $55 \pm 5\ \text{km/s}$ assuming the low-preshock density case of Hartigan, Morse, & Raymond (1994).

The comparison of the shock velocity, i.e., the relative velocity of the excited matter in the Herbig-Haro flow, to the flow speed of ~ 500 km/s implies that the HHO 494 does not represent the terminal shock.

The presence of the HHO indicates recent outflow activity and ongoing accretion. Indeed Launhardt & Sargent (2001) find indirect signatures of ongoing accretion and a possible disk wind. However, no large-scale molecular outflow has been detected so far which might be due the lack of sufficiently dense molecular gas in and around this nearly dispersed globule.

No HHO was found for the counter flow within 20' south-east of CB 26 YSO 1. This is presumably due to the low density of the ambient matter which precludes shock formation. The wide-field optical images show this area to be devoid of any globule remnants, contrary to the region north-west of the source.

5. Summary and conclusions

We report high-resolution NIR observations of a YSO in the Bok globule CB 26. Launhardt & Sargent (2001) obtained subarcsecond-resolution mm images of this source which they interpreted in terms of a young, large, and massive protoplanetary disk of mass $\approx 0.1 M_{\odot}$ surrounded by a remnant envelope of mass $\approx 0.1 M_{\odot}$. From the rotation curve of the disk they deduced a mass of the central star of $\approx 0.3 M_{\odot}$. Here we use NIR images and polarimetry of the reflection nebula to deduce the morphology of the envelope and the location and age of the central illuminating star. We also report the discovery of a Herbig-Haro flow from this source and derive further constraints on the morphology and evolutionary stage of the YSO-disk-envelope system. The main results are summarized as follows:

1. The NIR reflection nebula has a bipolar shape and is bisected by an extinction lane due to an edge-on seen circumstellar disk. The two lobes are due to light from the obscured central star scattered at grains in the envelope below and above the disk. The non-uniform extinction by either an irregular shape of the remnant envelope or a foreground filament prevents the derivation of the exact inclination angle from the NIR images.
2. The very small value of the disk inclination suggested by the mm results ($\lesssim 5^{\circ}$) is inconsistent with the estimate based on the velocity components of the Herbig-Haro flow ($\gtrsim 18^{\circ}$). This discrepancy might be solved by invoking a precession of the flow, e.g. due to a binary star or other mechanisms (Fendt & Zinnecker 1998). Settling the issue of the disk inclination requires observations at higher spatial resolution and the application of 2D/3D radiative transfer models.

3. A centro-symmetric polarization pattern and very high polarization degree of $p \sim 50 \dots 90\%$ indicates the presence of a single illuminating object. From the polarization pattern, its location is derived to be at the center of the extinction lane and disk. The object can be a single star or a close binary.
4. From the bolometric luminosity obtained by integrating the SED between $\lambda = 0.9 \mu\text{m}$ and 3 mm , the mass of the central star derived from the rotation curve of the disk, and using the PMS evolutionary tracks of Siess et al. (2000), we derive an upper limit for the age of the system of 10^6 yr .
5. Evidence for ongoing accretion and outflow activity comes from the discovery of HHO 494 which is well aligned with the symmetry axis of the mm disk. The outflow velocity of 160 km/s implies a dynamical time-scale of 1600 yr . The gas density of 200 cm^{-3} derived from the electron density and the ionization fraction is indicative for a low-density environment of the globule. No counterpart has been found for the redshifted flow.
6. CB26 YSO 1 is a classical Class I low-mass YSO, i.e., a star-disk system which has passed its main accretion phase but is still surrounded by a remnant envelope. Accretion from the envelope onto the disk and from the disk onto the star is still proceeding at low rates and outflow activity has not yet halted. The system is however distinguished by its extreme edge-on view, i.e., the symmetry axis is oriented very close to the plane of the sky. This prevents the detection of NIR and MIR emission from hot dust in the inner part of the disk.

CB26 YSO 1 resembles very closely both in appearance and physical parameters that of the Butterfly star in Taurus (IRAS 04302+2247; Wolf, Padgett, & Stapelfeldt 2003). Both objects are relatively isolated, have fairly large and massive circumstellar disks with signatures of grain growth, and are still associated with thin remnant envelopes. In contrast to the more evolved, smaller, and lower-mass TTS disks, these disks still accrete at low rates from the envelope, thus attaining the maximum mass and size during their evolution. We suggest that they represent the transition stage from embedded protostellar accretion disks to 'naked' protoplanetary disks around TTS in an undisturbed environment.

We thank R. Lenzen for his support during the MAGIC observations. O.F. and B.S. acknowledge travel grants from the Deutsche Forschungsgemeinschaft (DFG Fi 630/1-1, DFG Ste 605/7-1). This research has made use of the VizieR data base (Ochsenbein et al. 2000) and the NASA's Astrophysics Data System Bibliographic Services. The Second Palomar Observatory Sky Survey (POSS-II) was made by the California Institute of Technology

with funds from the National Science Foundation, the National Aeronautics and Space Administration, the National Geographic Society, the Sloan Foundation, the Samuel Oschin Foundation, and the Eastman Kodak Corporation.

REFERENCES

- André, P., Ward-Thompson, D., & Barsony, M. 1993, *ApJ*, 406, 122
- Bastien, P., & Ménard, F. 1990, *ApJ*, 364, 232
- Bally, J., Devine, D., & Alten, V. 1996, *ApJ*, 473, 921
- Bok, B.J. 1977, *PASP*, 89, 597
- Clemens, D.P., & Barvainis, R. 1988, *ApJS*, 68, 257
- Clemens, D.P., Yun, J.L., & Heyer, M.H. 1991, *ApJS*, 75, 877
- Condon, J.J., Broderick, J.J., Seielstad, G.A., Douglas, K., & Gregory, P.C. 1994, *AJ*, 107, 1829
- Czyzak, S.J., Keyes, C.D., & Aller, L.H. 1986, *ApJS*, 61, 159
- Elsässer, & H., Staude, H. J. 1978, *A&A*, 70, L3
- Feigelson, E.D., & Montmerle, Th. 1999, *ARA&A*, 37, 363
- Fendt, C., & Zinnecker, H. 1998, *A&A*, 334, 750
- Fischer, O., Henning, Th., & Yorke, H.W. 1994, *A&A*, 284, 187
- Guibert, J. 1992, *ASSL Vol. 174: Digitised Optical Sky Surveys*, 103
- Hartigan, P., Morse, J.A., & Raymond, J. 1994, *ApJ*, 436, 125
- Henning, Th., Wolf, S., Launhardt, R., & Waters, R. 2001, *ApJ*, 561, 871
- Herbst, T.M., Beckwith, S.V.W., Birk, Ch., Hippler, St. McCaughrean, M.J., Mannucci, F., & Wolf, J. 1993, in: *Infrared Detectors & Instrumentation*, *SPIE Proc. 1946*, ed. A.M. Fowler, 605
- Gregory P.C., Scott W.K., Douglas K., & Condon J.J. 1996, *ApJS*, 103, 427
- Kim, S.-H., Martin, P. G., & Hendry, P. D. 1994, *ApJ*, 422, 164

- Launhardt, R. 2001, IAU Symposium, 200, 117
- Launhardt, R., & Henning, Th. 1997, A&A, 326, 329
- Launhardt, R., Evans, Neal J.II, Wang, Y., Clemens, D.P., Henning, Th., & Yun, J.L. 1998, ApJS, 119, 59
- Launhardt, R., & Sargent, A.I. 2001, ApJ, 562, L173
- Leung, C.M. 1985, in: Protostars & Planets II, eds. D.C. Black & M.S. Matthews, University of Arizona Press, 104
- Men'shchikov, A.B., & Henning, Th. 1997, A&A, 318, 879
- Monet, D. et al. 1996, USNO-SA2.0, (U.S. Naval Observatory, Washington DC)
- Ochsenbein F., Bauer P., & Marcout J. 2000, A&AS, 143, 221
- Ossenkopf, V., & Henning, Th. 1994, A&A, 291, 943
- Padgett, D.L., Brandner, W., Stapelfeldt, K.R., Strom, S.E., Terebey, S., & Koerner, D. 1999, AJ, 117, 1490
- Pfeffermann, E., Aschenbach, B., & Predehl, P. 1991, A&A, 246, L28
- Raga, A.C., Böhm, K. H., Cantó, J. 1996, Rev. Mex. Astron. Astrofis. 32, 161
- Reipurth, B., Raga, A. C., & Heathcote, S. 1992, ApJ, 392, 145
- Reipurth, B. 1999, A general catalogue of Herbig-Haro objects, 2. edition, <http://casa.colorado.edu/hhcat>
- Reipurth, B. & Bally, J. 2001, ARA&A, 39, 403
- Rieke, G. H., Lebofsky, M. J. 1985, ApJ, 330, L33
- Scarrott, S.M., & Rolph, C.D. 1991, MNRAS, 249, 131
- Siebenmorgen, R., Kruegel, E., & Mathis, J. S. 1992, A&A, 266, 501
- Siess, L., Dufour, E., & Forestini, M. 2000, A&A, 358, 593
- Whitney, B.A., & Hartmann, L. 1993 ApJ, 402, 605
- Wolf, S., Padgett, D. L., & Stapelfeldt, K. R. 2003, ApJ, 588, 373

Yun, J.L., & Clemens, D.P. 1994, ApJS, 92, 145

Zinnecker, H. et al. 1999, A&A, 352, L73

Table 1. NIR-Photometry of CB26 IRS 1

Filter	Central Wavelength [μm]	Aperture [$''$]	FWHM [$''$]	F_ν [mJy]	σF_ν [mJy]	Comments
I	0.90	24	4.0	0.062	0.019	
J	1.25	12	0.9	2.2	0.2	
H	1.65	12	2.0	8.2	0.8	
Ks	2.16	12	1.9	17.1	1.7	
L'	3.77	6	2.1	28.5	14.0	size $3''.5 \times 2''.8$ at P.A. 130°

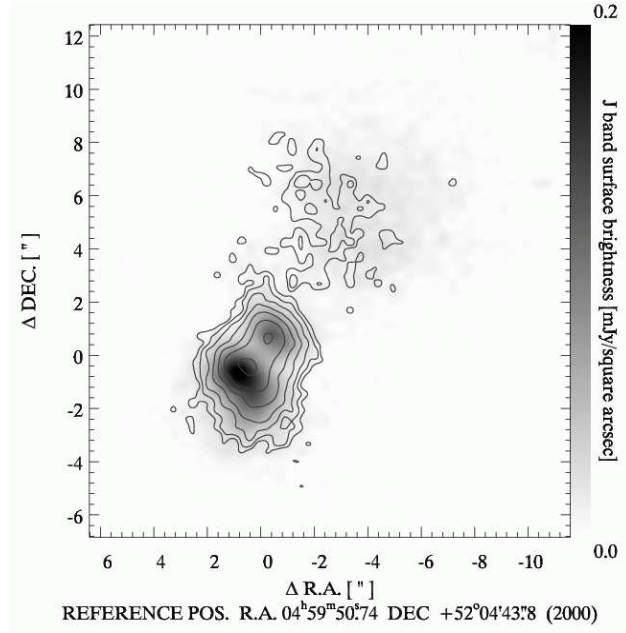


Fig. 1.— J-band image of CB 26 IRS 1 with contours of the K emission (levels are 0.14, 0.22, 0.34, 0.54, 0.86, 1.36, and 2.15 mJy/arc^2). The shift of the brightness peaks between J to K is due to the reduced optical depth at longer wavelength.

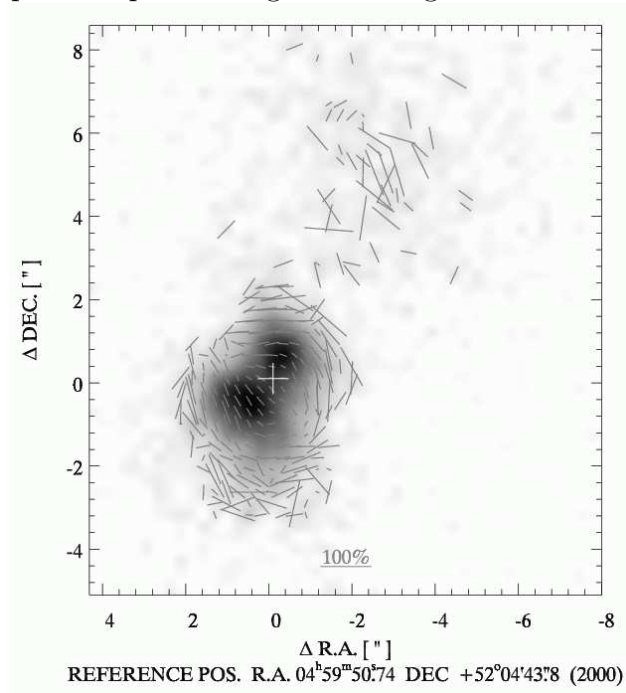


Fig. 2.— K-band image of CB 26 IRS 1 with superimposed vectors of the linear polarization (the horizontal bar marks $p = 100\%$). The white cross (at the reference position) marks the

most likely location of the illuminator and its size represents the positional uncertainty.

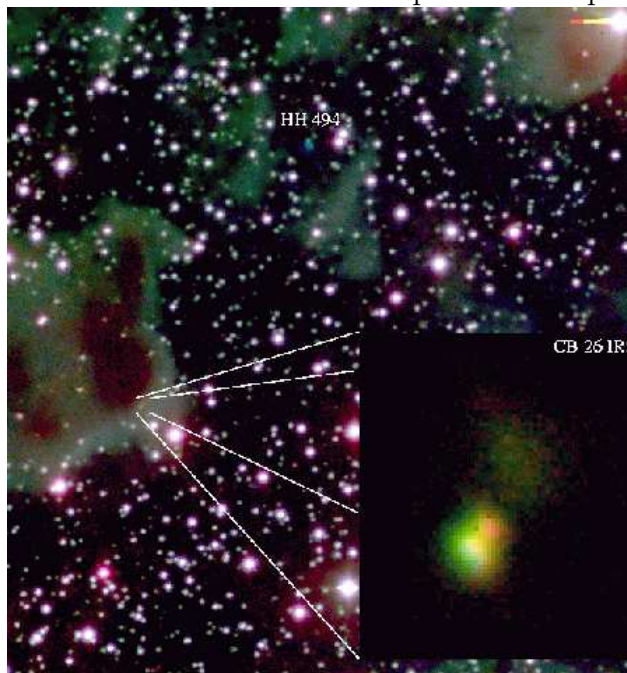


Fig. 3.— Color representation of the CB 26 region with IRS 1 as inset. The optical image is based on the $H\alpha$ (blue), [SII] (green), and I-band (red) frames while J, H, and K-band images were used for IRS 1. The HHO is marked in the optical image. In the near-infrared color composite, the mm-disk appears as brownish lane at the waist of the bipolar nebula.

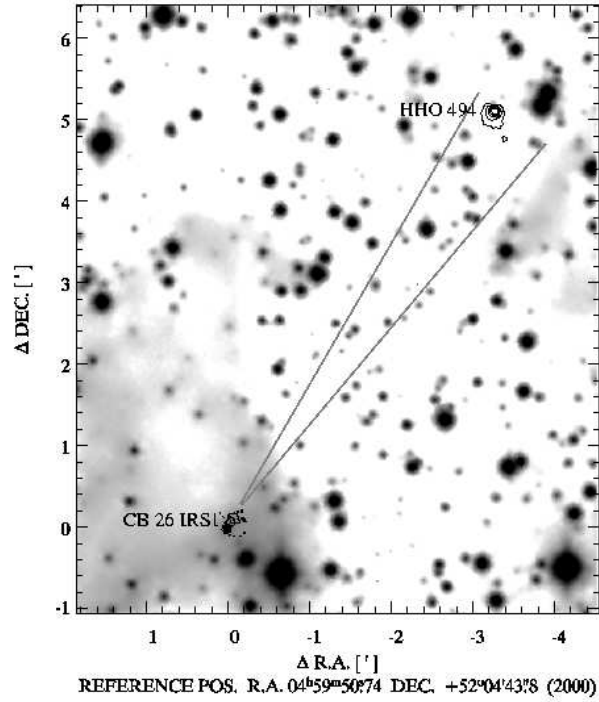


Fig. 4.— Wide-field I-band image of CB 26 and its surroundings (gray-scale). Overlaid are contours of the continuum-subtracted $H\alpha$ image (HHO 494) and of the J-band image of CB 26 IRS 1 (located at the reference position). The gray lines represent the symmetry axes error cone of CB 26 IRS 1 (see Sect. 3).

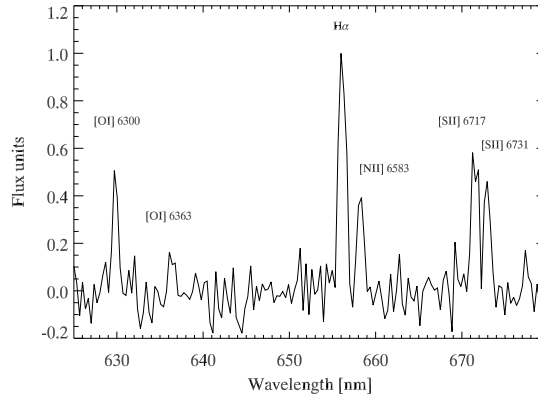


Fig. 5.— Spectrum of HHO 494 in the region of the $H\alpha$ line. Line fluxes are normalized to that of $H\alpha$. Prominent emission lines are marked.

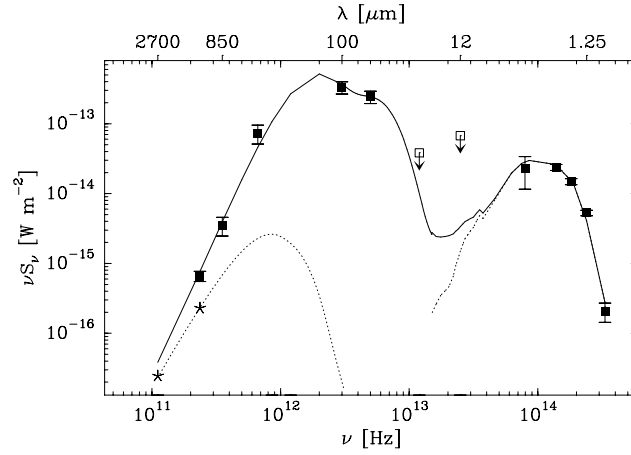


Fig. 6.— SED of CB 26 IRS 1. Full squares represent flux densities from the present paper, Launhardt & Henning (1997), Henning et al. (2001), Launhardt et al. (in prep.), and IRAS PSC. The upper limits of IRAS at 12 and 25 μm are marked by open squares. Asterisks represent the submm/mm fluxes for the disk only. The solid line represents the model, contributions from the disk and the stellar photosphere are indicated by dotted lines.